ABNUS JOURNAL
Your Research Partner

Jurnal Teknika dan Informatika (JTI)
E-ISSN: 2797-0000 | Vol. 1, No. 1 (2021) | pp. 46–61

Analysis of Frictional Energy Generation Between Train Wheels and Rails

Angganda Berlian Rms[1*], Erfiana Wahyuningsih[2]

[1,2] *Faculty of Engineering and Informatics, Mechanical Engineering Study Program, Dian Nusantara University, Jakarta, Indonesia*

***Corresponding author:** angganda.rms@undira.ac.id |

Received: 3 March 2021 | Revised: 15 April 2021 | Published: 16 May 2021

Abstract

Purpose: This study aims to analyze the friction between two homogeneous materials, specifically focusing on the friction between train wheels and rails during braking, and the energy produced by this friction that can potentially be utilized as renewable energy.
Research Methodology: A braking model was designed using a Direct Current (DC) motor as the driving force for the train. The frictional force (Fk) during braking was measured using an Arduino Mega control system that processed data from a speed sensor. The temperature changes resulting from friction were recorded and converted into energy. The experiment was conducted with different masses to evaluate the relationship between the load and energy produced from friction.
Results: The results show a significant linear correlation between friction force and energy production with an R^2 value of 0.9541. The maximum energy generated during braking, with a friction force of 1.864 Newtons, was 37.31 Joules.
Conclusions: This study demonstrates that energy generated from friction during braking could be harnessed as renewable energy. The results confirm that increased load and friction lead to higher energy output, showing the potential for more sustainable energy systems in transportation.
Limitations: The research was limited to specific materials and experimental conditions. Further studies are needed to explore different materials and environmental factors.
Contributions: This study contributes to the understanding of energy harvesting through friction, proposing a new avenue for sustainable energy sources in the transportation sector.

Keywords: *Arduino, Energy, Friction, Renewable Energy, Sustainable Transportation*

How to Cite: Berlian Rms, A., & Wahyuningsih, E.(2021). Analysis of Frictional Energy Generation Between Train Wheels and Rails. *Jurnal Teknika dan Informatika (JTI)*, *1*(1), 46–61. https://doi.org/10.52909/jti.v1i1.10

1. Introduction

The Jabodetabek Electric Rail Train (KRL) has undergone significant development as one of the main modes of land transportation in Indonesia. Since its service upgrade to Commuter Line in 2011, the KRL system has played an increasingly important role in supporting urban mobility, particularly in densely populated areas such as Jakarta, Bogor, Depok, Tangerang, and Bekasi (Prasodjo, 2019; Siburian et al., 2020). According to data from the Central Statistics Agency, the number of KRL users has increased substantially, from 8,774 passengers in 2006 to 27.7 million passengers in 2017. This rapid growth reflects the increasing dependence of the community on efficient and affordable public transportation systems.

The increase in the number of passengers directly affects the operational performance of the trains.

Higher passenger loads result in increased mass of the train carriages, which in turn influences train dynamics such as speed, acceleration, and braking performance (Cole et al., 2017). One of the most critical aspects affected by this condition is the braking system. As the load increases, the braking force required to stop the train also increases, leading to greater friction between mechanical components such as brake blocks, wheels, and rails (Cheli et al., 2017).

Friction is a fundamental physical phenomenon that occurs when two surfaces come into contact and move relative to each other. In the case of train braking systems, friction occurs between the brake blocks and the wheels, as well as between the wheels and the rails. This friction converts kinetic energy into thermal energy, resulting in a rise in temperature at the contact surfaces (Dou & Subotnik, 2018; Marques et al., 2019; Milton et al., 2016). In many cases, the heat generated is significant enough to produce visible sparks, particularly during intense braking conditions. In addition to heat, friction also generates noise, which can contribute to environmental pollution and negatively impact human health, especially hearing (Günay et al., 2020; Sharma & Kumar, 2018).

The quality and material properties of brake components, such as brake blocks, also influence the magnitude of friction, heat generation, and noise levels (Li et al., 2020). Poor-quality materials may increase wear, reduce braking efficiency, and amplify noise emissions. Therefore, understanding the interaction between materials and frictional forces is essential for improving the performance and safety of railway systems (Tang et al., 2019).

Despite the fact that frictional heat is generally considered as wasted energy, it actually presents an opportunity for energy recovery and utilization (Xiang et al., 2020). The heat energy generated during braking has the potential to be converted into useful energy, contributing to the development of New and Renewable Energy (NRE) sources (Björnsson & Karlsson, 2016). With the growing global demand for sustainable energy solutions, exploring alternative energy sources from existing mechanical processes has become increasingly important.

Train braking systems typically use compressed air and automatic compressed air mechanisms to control deceleration (Hoxha et al., 2017). During braking, the conversion of kinetic energy into heat energy is unavoidable. However, instead of allowing this energy to dissipate into the environment, it can be harnessed and converted into other forms of energy. This concept aligns with the broader effort to improve energy efficiency and reduce energy losses in transportation systems (Zhao et al., 2019).

In addition to friction-induced heat, the operation of trains also involves other energy-related aspects, such as the use of direct current (DC) motors (Bürklein et al., 2019; Ferreira et al., 2017). The speed of DC motors can be controlled by adjusting the direction and magnitude of their rotational motion, either clockwise (CW) or counterclockwise (CCW). This capability highlights the potential integration of mechanical and electrical systems in energy conversion processes (Chen et al., 2020; Parihar et al., 2016; Sigalos et al., 2019).

Based on these considerations, the problem identified in this study is that braking in electric trains creates continuous friction between wheels and rails, which generates heat energy that is currently underutilized. This continuous friction represents a potential source of renewable energy if it can be effectively captured and converted. Therefore, this research focuses on modeling the friction between two homogeneous metal objects representing train wheels and rails (Dağdelen & Sarıgeçili, 2020; Kishor & Singh, 2017).

The purpose of this study is to analyze the frictional force between similar metal materials and to estimate the amount of energy produced as a result of friction. Furthermore, this study aims to establish a correlation between theoretical friction coefficients and real-world conditions. The results of this research are expected to contribute to the development of alternative energy technologies and provide a foundation for further studies in the field of New and Renewable Energy (NRE), particularly in the

context of transportation systems.

2. Literature Review

Braking on a commuter train involves metal parts such as brake blocks, wheels, and rails/train tracks. The frictional force during braking (wheel with brake) and (wheel with rail) causes temperature changes (Handa et al., 2020; Walia et al., 2019). Temperature changes can be converted into energy sources. This case study requires supporting libraries to create an analysis of frictional forces as an energy source. The model uses a DC motor, Rotary Encoder sensor, Arduino Mega, and other components (Chen et al., 2019; Shrestha et al., 2019). The configuration of each device is studied and explored, including the following:

2.1 Relationship between Speed and Friction

Friction is a force that acts opposite to the motion or tendency of motion of an object. Friction occurs when two solid objects are in contact. Static friction and kinetic friction are two types of friction (Tonazzi et al., 2018; Wójcik et al., 2020). Kinetic friction (F_k) occurs when two objects move relative to each other and rub together.

$$F_k = \mu_k \cdot N$$

Where:

- F_k = Maximum kinetic friction force (Kgf or N)
- μ_k = Coefficient of kinetic friction (dimensionless)
- N = Normal force

The wheels of the train rotate with a certain radius, and there is a centrifugal force acting on the train. The following is the equation for the centrifugal force (linear) on the train:

In addition to centrifugal force, the wheels of the train experience rotational force, given by:

$$F = k \cdot m \cdot \omega^2$$

$$F = \frac{mv^2}{R}$$

Considering the translational motion of a ball moving in a straight line, with the assumption that all external forces act at the center of mass, Newton's second law becomes:

$$\Sigma F_x = ma, \quad F - F_k = ma, \quad F - F_k = I\alpha$$

Where:

- F = Force (N)
- ω = Angular velocity (rad/s)
- m = Mass (kg)
- I = Moment of inertia (kg m^2)
- v = Linear speed (m/s)

- k = Inertial Constant
- R = Radius (m)
- α = Angular acceleration (rad/s^2)

2.2 Thermal Conductivity with Energy

The thermal conductivity of a material is a measure of the material's ability to conduct heat (thermal), and the thermal conductivity value of a material indicates the rate of heat transfer (Kumanek & Janas, 2019; Pryazhnikov et al., 2017). For example, a sheet of plate has a cross- section A and a thickness of ÿx, and the two surfaces are maintained at different temperatures (Asadi et al., 2018; Sargam et al., 2020). The heat Q flowing perpendicular to the surface during time t was measured.

$$\frac{Q}{t} = \frac{kA(T_2 - T_1)}{L}$$

Where:

- Q = Energy (J)
- k = Thermal conductivity (W/m °C)
- t = Time (s)
- T = Temperature (°C)
- A = Cross-sectional area (m^2)
- L = Length (m)

2.3 Rotary Encoder Sensor

The Rotary Encoder (Figure 2.1) detects the motor speed. The resulting pulses represent dark/black (high voltage) and light/white (low voltage) spaces. These pulses indicate motor movement, which is detected through the gaps in the disc of the Rotary Encoder sensor module.

Image caption:
A = dark gap of the Rotary Encoder disc
B = bright gap of the Rotary Encoder disc

Figure 1. Total Cooling Load Graph

Based on Figure 1, the image shows a rotary encoder system, which consists of a rotating disk (on the right) and the sensor mechanism (on the left). As the disk rotates, it passes through the sensor, creating

alternating light and dark gaps. These changes in light intensity trigger a digital pulse output from the sensor, which is then used to detect the position or rotation of the disk. The sensor detects the transition from light to dark and vice versa, generating pulses that can be interpreted as rotational data for further processing in a control system.

2.4 The Arduino Mega

minimum microcontroller system is compatible and flexible with the open source Integrated Development Environment (IDE) software. The Arduino Mega is programmed with the IDE software , and the programming results are uploaded to the microcontroller's memory.

2.5 The LCD Data

The display is a dot matrix display for displaying text in the form of numbers or letters. The letter characters and numbers on the LCD screen make it easier to convey certain information.

2.6 PIR (Passive Infrared) Sensor

A passive infrared (PIR) sensor detects temperature. As the name suggests, this sensor is passive in nature. It receives infrared signals emitted by an object (in this case, a solid object). Currently, there are many types of PIR sensors available in the market.

The characteristics of the PIR sensor are as follows:

1. Operating voltage 4.7 – 10 Volts
2. Measurement resolution is 0.02°
3. Detected temperature between -70 – 38°
4. Detection range 5 meters
5. Detection speed 0.5 seconds

3. Methodology

Research methodology refers to the stages of research that must be established before problem-solving can be undertaken. This allows for focused research and facilitates the analysis of problems. The following flowchart of the research method used is shown in Figure 2.

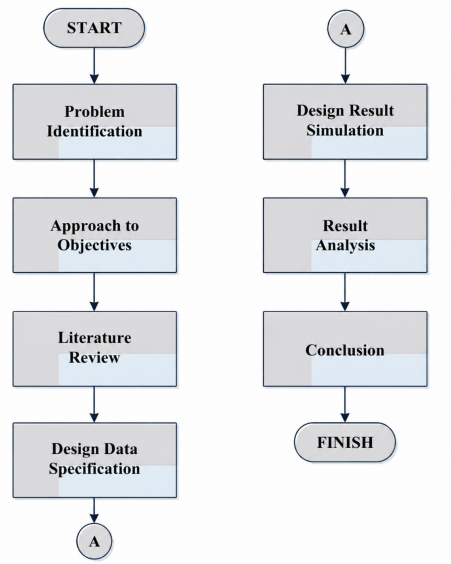

Figure 2. Research Flowchart

Based on Figure 2, the flowchart outlines a step-by-step process in a two-column structure. The left column begins with the "START" phase, followed by steps such as "Problem Identification," "Approach to Objectives," "Literature Review," and "Design Data Specification." The right column progresses from "A" to the final "FINISH" stage, including "Design Result Simulation," "Result Analysis," and "Conclusion." The flowchart clearly shows the sequential steps required for the process and the interconnections between each stage.

3.1 Data Collection Procedure

In this study, the friction between the train wheels and rails was supported by an appropriate braking model. Motor 1 was modeled as a wheel with a higher RPM than that of motor 2, which acted as a brake. Accuracy and careful planning are essential in designing the train's braking system. Electronic components are integrated, and program instructions were inserted into the system controller as designed.

3.2 Data Specifications and Calculations

The data specifications used were quantitative with discrete data. The data are presented in two tables: speed sensor testing table and temperature sensor testing table. Speed sensor testing table with columns; constant voltage (v) input motor 1 and 2, RPM motor 1, RPM motor 2, tachometer motor 1 (RPM), tachometer motor 2 (RPM), speed motor 1 (v) m/s, speed motor 2 (v) m/s and friction force (Fk). Temperature sensor testing table with columns: RPM 1, RPM 2, constant braking time (s) at various speed values, temperature sensor (T0 and T1), temperature detected by thermometer (T0 and T1), error value, and energy. The following is a construction drawing of the train braking model (Figure 3).

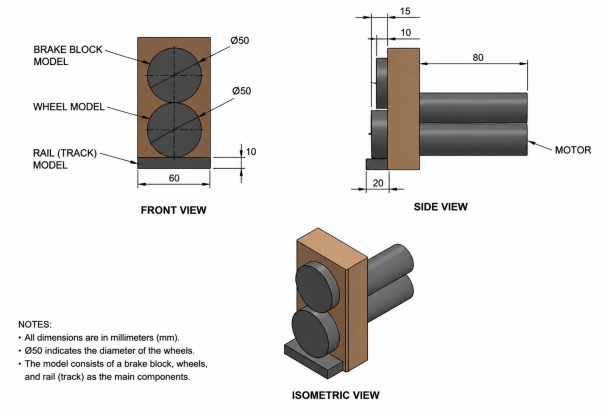

Figure 3. Research Flowchart

Based on Figure 3, the diagram illustrates a technical design of a brake system model. It includes three views: the front view, side view, and isometric view. The front view shows the brake block, wheels, and track with labeled dimensions, including the diameter of the wheels (Ø50) and the total width of the model. The side view provides a perspective with additional details on the motor placement and the overall length of the assembly. The isometric view offers a 3D visualization of the complete model. Notes at the bottom clarify that all dimensions are in millimeters, with the model consisting of the brake block, wheels, and track as the primary components.

3.3 Speed Sensor Test Results

Table 1. Results of Rpm Value Measurement

Time (s)	Input Voltage (V)	Clockwise (CW)		Counter Clockwise (CCW)	
		RPM Motor 1	RPM Motor 2	RPM Motor 1	RPM Motor 2
0	0	0	0	0	0
5	3	75	40	75	40
10	3	74	41	75	41
15	6	167	86	167	86
20	6	167	84	167	85
25	9	250	131	250	131
30	9	249	133	250	133
35	10	278	148	278	148
40	10	277	146	277	146
45	12	334	178	333	178
50	12	334	177	334	178
55	14	399	211	398	211
60	14	399	211	399	211

Based on Table 1, it can be seen that the motor speed increases as the input voltage rises, demonstrating a direct relationship between voltage and rotational speed. Additionally, the RPM values for both clockwise (CW) and counterclockwise (CCW) directions show similar trends, suggesting that the system operates symmetrically under both rotational conditions.

Table 2. Speed Measurement Results

No.	Input (V)	M1 (RPM)	M2 (RPM)	Tach 1 (RPM)	Tach 2 (RPM)	v1 (m/s)	v2 (m/s)	Fk (N)
1	3	75.1	40.0	74.8	39.7	0.197	0.105	0.168
2	3	74.9	40.0	74.6	40.1	0.196	0.105	0.167
3	6	167.1	86.1	167.2	86.2	0.437	0.225	0.845
4	6	167.1	84.3	167.1	84.1	0.437	0.221	0.853
5	9	250.3	131.3	250.1	130.9	0.655	0.344	1.879
6	9	250.2	133.1	250.0	132.9	0.655	0.348	1.864
7	10	277.7	148.1	278.1	148.2	0.727	0.388	2.294
8	10	277.9	146.7	277.3	146.5	0.727	0.384	2.309
9	12	334.2	178.3	333.9	177.9	0.874	0.467	3.321
10	12	334.4	177.1	334.3	177.1	0.875	0.463	3.338
11	14	398.8	210.6	398.7	210.2	1.044	0.551	4.755
12	14	399.1	210.6	399.0	211.0	1.044	0.551	4.764

Based on Table 2, it can be observed that the increase in input voltage significantly affects the motor performance parameters. As the voltage rises from 3 V to 14 V, both motor speeds (M1 and M2) and tachometer readings show a consistent increase. This indicates a direct relationship between input voltage and rotational speed. In addition, the linear velocities (v1 and v2) also increase proportionally with motor speed, reflecting the conversion of rotational motion into linear motion. Furthermore, the friction force (Fk) increases as the speed and velocity increase, demonstrating that higher motion intensity leads to greater frictional interaction between the contact surfaces. Overall, the data show a stable and consistent trend between voltage, speed, velocity, and friction force, which supports the theoretical relationship between these variables.

The following explanation regarding the calculations for the correlation value analysis is presented in the following table:

Table 3. Friction Coefficient Correlation Values

No	x (v1 m/s)	y (Fk N)	x^2	y^2	xy
1	0.197	0.048	0.039	0.002	0.009
2	0.196	0.047	0.038	0.002	0.009
3	0.437	0.249	0.191	0.062	0.109
4	0.437	0.257	0.191	0.066	0.112
5	0.655	0.542	0.429	0.294	0.355
6	0.655	0.529	0.429	0.280	0.346
7	0.727	0.648	0.528	0.420	0.471
8	0.727	0.661	0.529	0.437	0.481
9	0.874	0.938	0.765	0.881	0.821
10	0.875	0.952	0.766	0.906	0.833
11	1.044	1.361	1.089	1.852	1.420
12	1.044	1.365	1.091	1.862	1.425
Total	7.868	7.597	6.084	7.064	6.392

Based on Table 3, it can be observed that there is a strong positive relationship between velocity (v_1) and friction force (F_k). As the velocity increases, the friction force also increases significantly. This trend indicates that higher motion speed leads to greater frictional interaction between the contact surfaces. Additionally, the values of x^2, y^2, and xy show consistent growth, supporting the existence of a linear

correlation between the variables. The total values further confirm the proportional relationship, which can be used for regression analysis to determine the coefficient of friction and energy characteristics of the system. The results of the calculation show that there is a relationship between the speed and friction. 2 = 0.9541 means that speed affects the friction by 95.41%.

3.4 Temperature Sensor Test

Results: The temperature was influenced by the speed and duration of the DC motor rotation. The linear speed is influenced by the RPM, wheel circumference, and additional load. Solid iron with varying masses was used as the load for motor rotation. The temperature detected by the PIR sensor was compared with that measured using a thermometer.

Table 4. Temperature Measurement Results

No	M1 (RPM)	M2 (RPM)	Time (s)	Temperature Sensor (°C)		Thermometer (°C)		Error (%)		ΔT (°C)	Energy (J)
				T_0	T_1	T_0	T_1	T_0	T_1		
1	75.1	40	29.87	32.3	32.72	32.5	32.92	1%	1%	0.42	33.34
2	74.9	40	29.87	32.3	32.73	32.5	32.93	1%	1%	0.43	34.14
3	167.1	86.1	29.87	32.4	32.84	32.6	33.04	1%	1%	0.44	34.93
4	167.1	84.3	29.87	32.5	32.95	32.8	33.25	1%	1%	0.45	35.73
5	250.3	131.3	29.87	32.6	33.06	32.9	33.36	1%	1%	0.46	36.52
6	250.2	133.1	29.87	32.6	33.07	32.9	33.37	1%	1%	0.47	37.31
7	277.7	148.1	29.87	32.7	33.18	33.0	33.48	1%	1%	0.48	38.11
8	277.9	146.7	29.87	32.9	33.39	33.3	33.79	1%	1%	0.49	38.90
9	334.2	178.3	29.87	32.9	33.41	33.3	33.81	1%	1%	0.51	40.49
10	334.4	177.1	29.87	33.1	33.62	33.5	34.02	1%	1%	0.52	41.28
11	398.8	210.6	29.87	33.1	33.63	33.5	34.03	1%	1%	0.53	42.08
12	399.1	210.6	29.87	33.2	33.74	33.7	34.24	1%	1%	0.54	42.87

Based on Table 4, it can be observed that the increase in motor speed (M1 and M2) results in a gradual increase in temperature, both in the sensor readings and thermometer measurements. The temperature difference (ΔT) also increases consistently, indicating that higher rotational speeds generate more heat due to friction. Furthermore, the calculated energy values show a proportional increase with temperature change, confirming that frictional heat contributes to energy generation. The error values remain constant at 1%, indicating that the measurement system is relatively stable and reliable. Overall, the data demonstrate a direct relationship between rotational speed, temperature rise, and generated energy.

Table 5. Braking Distance Measurement

Initial Velocity (v_0) (km/h)	Braking Distance (l) (m)
60	249
70	332
80	420
90	527
100	650

Based on Table 5, it can be observed that the braking distance increases significantly as the initial velocity (v_0) increases. When the velocity rises from 60 km/h to 100 km/h, the braking distance increases from 249 m to 650 m. This indicates a nonlinear relationship between velocity and braking distance, where higher speeds result in a much longer stopping distance. The results suggest that kinetic energy and inertia play a major role in braking performance, requiring greater distance to dissipate energy through friction.

4. Results and Discussion

4.1 Analysis of CW/CCW Motor RPM Data

The following is a graph of the tested motor RPM values in the anti-clockwise (CCW) and clockwise (CW) directions:

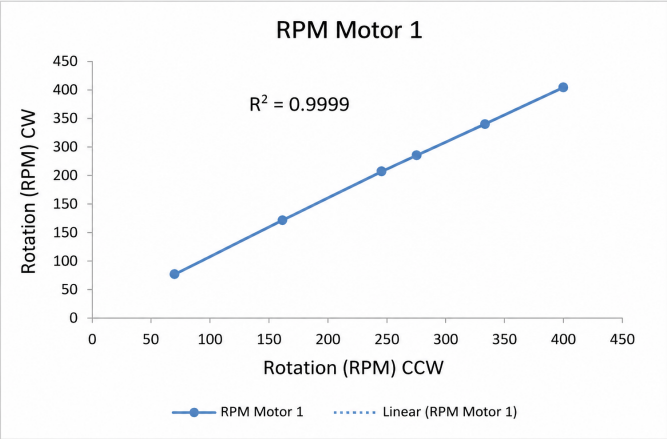

Figure 4. Graph of Motor RPM Values 1

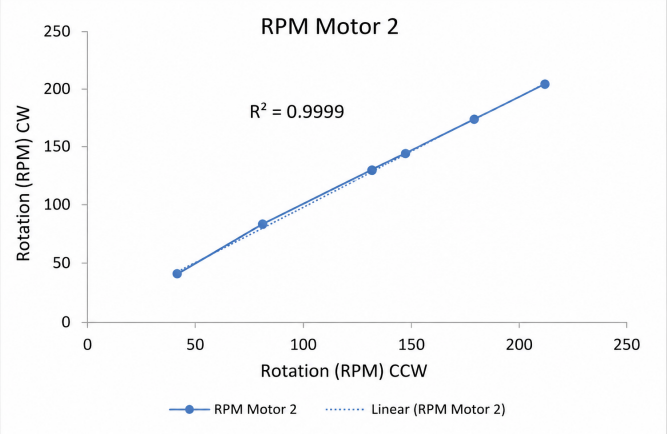

Figure 5. Graph of Motor RPM Values 2

Based on Figure 4 and Figure 5, it is observed that when motor 1 rotates in the CW or CCW direction, it produces the same RPM value. Likewise, the graph of the RPM value of motor 2. This can be proven using the correlation method. If the results of the correlation coefficient show an R2 value ranging from $0.8 < R2 < 1$ then the two variables are closely related (Ayyasy, ELINVO 2016, 5), the RPM value of the CW direction is in accordance with the CCW with $R2 = 0.9$.

4.2 Analysis of Friction Force Data Against Variations in Mass Load

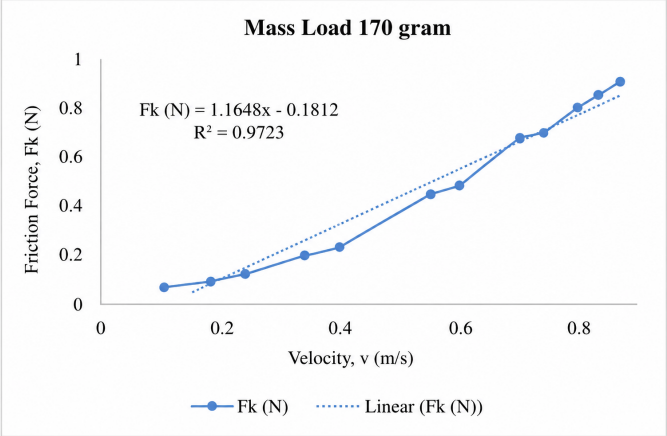

Figure 6. Correlation Graph of Friction Force on a 170 gr Load

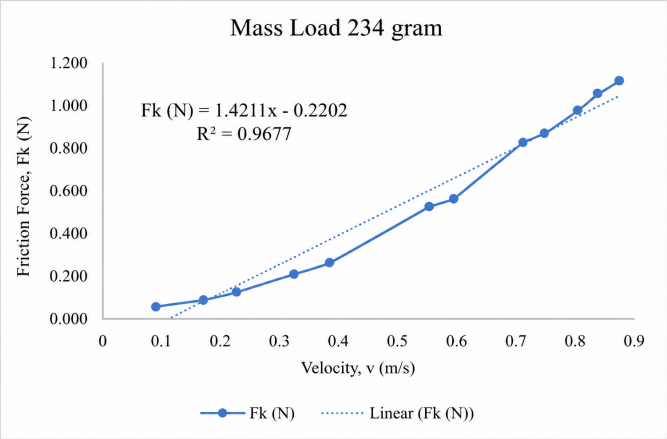

Figure 7. Correlation Graph of Friction Force on a 234 gr Load

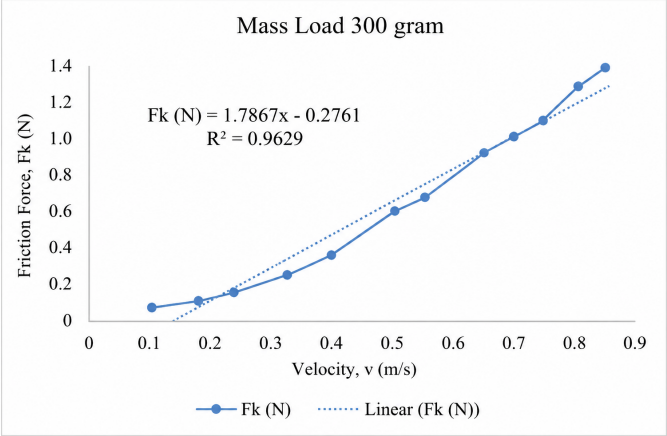

Figure 8. Correlation Graph of Friction Force on a 300 gr Load

Based on Figure 6, Figure 7, and Figure 8, the difference in the friction force influenced by speed and mass load is observed in the results of the correlation calculation. A 170 g mass load had the equation Fk = 1.1648x - 0.1812, a 234 g mass load had the equation Fk = 1.4211x - 0.2202, and a 300 g mass load had the equation Fk = 1.7867x - 0.2761. Therefore, under the same speed condition, the friction force has a large value for a heavier mass load. The R2 correlation values show that in the range 0.8 < R2 < 1, there is a relationship between the motor speed and frictional force. The speed is directly proportional to the frictional force. After obtaining the rate of heat absorption from the water and the walls of the induction furnace, the total heat absorption was calculated the heat absorption was 0.29 kW.

Information: Fk = Friction Force (N) and x = v = Motor Speed (m/s)

4.3 Temperature Sensor Data Analysis

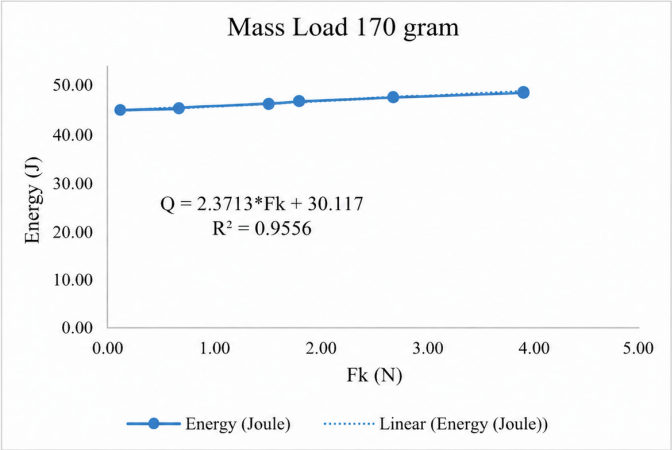

Figure 9. Graph of the Relationship between Frictional Force and Energy 1

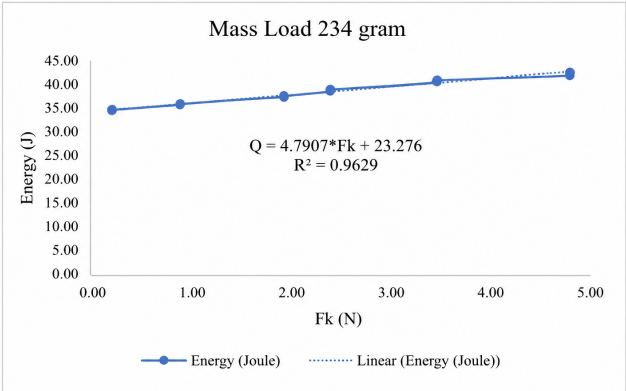

Figure 10. Graph of the Relationship between Frictional Force and Energy 2

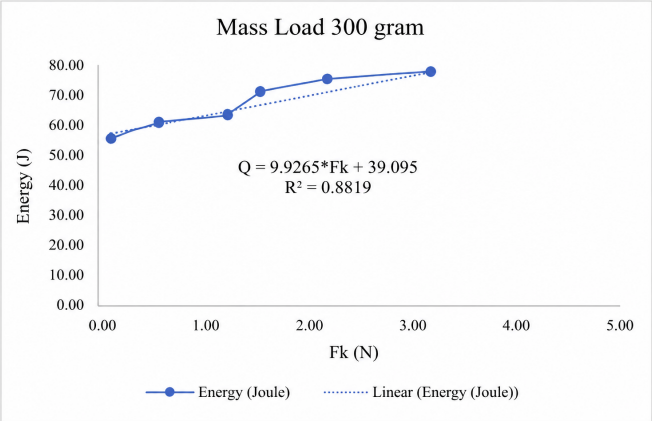

Figure 11. Graph of the Relationship between Frictional Force and Energy 3

Based on Figure 9, Figure 10, Figure 11, the amount of energy affected by friction and mass load can be observed in the results of the correlation calculation. A mass load of 170 grams has the equation: Q = 2.3713* Fk + 30.117. A mass load of 234 grams has the equation: Q = 4.7907* Fk + 23.276. For a mass load of 300 grams, the equation is: Q = 9.9265 * Fk + 39.095.

Description:

- Q = Energy (J)
- F_k = Frictional Force (N)

As shown in the graph above, the correlation value in Figure 9 indicates that the data results are linear, as $R^2 = 0.9556$. The most linear correlation value is shown in Figure 9. The difference in the correlation results is due to variations in the applied mass load. These graphs demonstrate that the greater the friction force value, the greater the energy generated.

5. Conclusions

The motor rotational speed was detected using a rotary encoder sensor and tested with a tachometer measuring instrument comparator. The rotation of motors 1 and 2 in opposite directions causes friction. The continuous friction between the track and solid causes temperature changes. Temperature changes detected on the railway track can be converted into energy. The temperature on the track was detected using an infrared temperature sensor and a digital thermometer for comparison.

From the results of the study, it can be concluded that:

1. The correlation value resulting from friction force and energy is between $0.8 < R^2 < 1$, so it can be said that the resulting data were linear. This is in accordance with the journal mentioned previously; if the test data are linear, then the friction force has a relationship with energy.
2. The results of this study prove that the frictional force that arises from the train's braking produces energy (Joules) that can be used for further energy utilization.
3. The solid is modeled as a load, and when the load is added, the energy produced increases. This can be correlated with the fact that if the load is passengers, then the energy produced from the additional passengers/load will be greater.
4. The frictional force generated is influenced by the speed of the motor. The higher the speed, the

greater is the frictional force.

5. The correlation value of the data was between $0.8 < R^2 < 1$. If the correlation result obtained is less than 0.8 or more than 1, the variables are not closely related.

Acknowledgements

The authors would like to express their gratitude to the Faculty of Engineering and Informatics, Dian Nusantara University, for their support throughout this study. Special thanks to the team at the Department of Mechanical Engineering for their valuable insights. The authors also acknowledge the assistance of the laboratory staff and all participants who contributed to the success of this research.

Author Contributions

ABR conceived the research idea and designed the methodology for the study. He conducted the experiments, analyzed the data, and was primarily responsible for writing the manuscript. EW supervised the project, offering valuable guidance and critical insights. She also reviewed the manuscript thoroughly, suggesting revisions and ensuring the overall quality of the work.

Conflicts of Interest

The authors declare that there is no conflict of interest regarding the publication of this study. This research was conducted independently, and no financial or personal relationships influenced the results or interpretation of the findings.

 DOI:10.52909/jti.v1i1.10

References

Asadi, I., Shafigh, P., Hassan, Z. F. B. A., & Mahyuddin, N. B. (2018). Thermal conductivity of concrete–a review. *Journal of Building Engineering*, *20*, 81–93. https://doi.org/10.1016/j.jobe.2018.07.002

Björnsson, L. H., & Karlsson, S. (2016). The potential for brake energy regeneration under swedish conditions. *Applied Energy*, *168*, 75–84. https://doi.org/10.1016/j.apenergy.2016.01.051

Bürklein, S., Stüber, J. P., & Schäfer, E. (2019). Real-time dynamic torque values and axial forces during preparation of straight root canals using three different endodontic motors and hand preparation. *International Endodontic Journal*, *52*(1), 94–104. https://doi.org/10.1111/iej.12980

Cheli, F., Di Gialleonardo, E., & Melzi, S. (2017). Freight trains dynamics: Effect of payload and braking power distribution on coupling forces. *Vehicle System Dynamics*, *55*(4), 464–479. https://doi.org/10.1080/00423114.2016.1246743

Chen, N., Zheng, J., Jiang, X., Fan, S., & Fan, D. (2020). Analysis and control of micro-stepping characteristics of ultrasonic motor. *Frontiers of Mechanical Engineering*, *15*(4), 585–599. https://doi.org/10.1007/s11465-019-0577-3

Chen, S., Zhao, G., Wang, H., Tao, G., Wen, Z., & Wu, L. (2019). Study of wheel wear influenced by tread temperature rising during tread braking. *Wear*, *438*, 203046. https://doi.org/10.1016/j.wear.2019.203046

Cole, C., Spiryagin, M., Wu, Q., & Sun, Y. Q. (2017). Modelling, simulation and applications of longitudinal train dynamics. *Vehicle System Dynamics*, *55*(10), 1498–1571. https://doi.org/10.1080/00423114.2017.1330484

Dağdelen, M., & Sarıgeçili, M. (2020). An experimental method for estimating combined friction torque in vane type pneumatic semi rotary actuators. *Sakarya University Journal of Science*, *24*(6), 1272–1283. https://doi.org/10.16984/saufenbilder.652782

Dou, W., & Subotnik, J. E. (2018). Perspective: How to understand electronic friction. *The Journal of Chemical Physics*, *148*(23). https://doi.org/10.1063/1.5035412

Ferreira, F., Adeodato, C., Barbosa, I., Aboud, L. R. D. L., Scelza, P., & Zaccaro Scelza, M. (2017). Movement kinematics and cyclic fatigue of niti rotary instruments: A systematic review. *International Endodontic Journal*, *50*(2), 143–152. https://doi.org/10.1111/iej.12613

Günay, M., Korkmaz, M. E., & Özmen, R. (2020). An investigation on braking systems used in railway vehicles. *Engineering Science and Technology, an International Journal*, *23*(2), 421–431. https://doi.org/10.1016/j.jestch.2020.01.009

Handa, K., Ikeuchi, K., & Morimoto, F. (2020). Temperature-dependent wear of tread-braked railway wheels. *Wear*, *452*, 203265. https://doi.org/10.1016/j.wear.2020.203265

Hoxha, E., Habert, G., Lasvaux, S., Chevalier, J., & Le Roy, R. (2017). Influence of construction material uncertainties on residential building lca reliability. *Journal of Cleaner Production*, *144*, 33–47. https://doi.org/10.1016/j.jclepro.2016.12.068

Kishor, V., & Singh, M. S. (2017). Design and development of arduino uno based quadcopter. *International Journal of Engineering and Manufacturing Science*, *7*(1), 14–19.

Kumanek, B., & Janas, D. (2019). Thermal conductivity of carbon nanotube networks: A review. *Journal of Materials Science*, *54*(10), 7397–7427. https://doi.org/10.1007/s10853-019-03368-0

Li, W., Yang, X., Wang, S., Xiao, J., & Hou, Q. (2020). Comprehensive analysis on the performance and material of automobile brake discs. *Metals*, *10*(3), 377. https://doi.org/10.3390/met10030377

Marques, F., Flores, P., Claro, J. P., & Lankarani, H. M. (2019). Modeling and analysis of friction including rolling effects in multibody dynamics: A review. *Multibody System Dynamics*, *45*(2), 223–244. https://doi.org/10.1007/s11044-018-09640-6

Milton, K. A., Høye, J. S., & Brevik, I. (2016). The reality of casimir friction. *Symmetry*, *8*(5), 29. https://doi.org/10.3390/sym8050029

Parihar, P., Bhawsar, P., & Hargod, P. (2016). Design development analysis of quadcopter. *Compusoft*, *5*(6), 2128.

Prasodjo, H. (2019). The imports of used krl as indonesia's dependency on japan in electric train technology. *Global Local Interactions: Journal of International Relations*, *1*(2), 10–21.

Pryazhnikov, M. I., Minakov, A. V., Rudyak, V. Y., & Guzei, D. V. (2017). Thermal conductivity measurements of nanofluids. *International Journal of Heat and Mass Transfer*, *104*, 1275–1282. https://doi.org/10.1016/j.ijheatmasstransfer.2016.09.080

Sargam, Y., Wang, K., & Alleman, J. E. (2020). Effects of modern concrete materials on thermal conductivity. *Journal of Materials in Civil Engineering*, *32*(4), 04020058. https://doi.org/10.1061/(ASCE)MT.1943-5533.0003026

Sharma, S. K., & Kumar, A. (2018). Impact of longitudinal train dynamics on train operations: A simulation-based study. *Journal of Vibration Engineering & Technologies*, *6*(3), 197–203. https://doi.org/10.1007/s42417-018-0033-4

Shrestha, S., Spiryagin, M., & Wu, Q. (2019). Friction condition characterization for rail vehicle advanced braking system. *Mechanical Systems and Signal Processing*, *134*, 106324. https://doi.org/10.1016/j.ymssp.2019.106324

Siburian, T. E., Widyawati, W., & Shidiq, I. P. A. (2020). Characteristics of transit oriented development area (case study: Jakarta mrt). *Jurnal Geografi Lingkungan Tropik*, *4*(1), 46–58.

Sigalos, A., Papoutsidakis, M., Chatzopoulos, A., & Piromalis, D. (2019). Design of a flight controller and peripherals for a quadcopter. *International Journal of Engineering Applied Sciences and Technology*, *4*(5), 463–470. https://doi.org/10.33564/ijeast.2019.v04i05.067

Tang, B., Mo, J. L., Xu, J. W., Wu, Y. K., Zhu, M. H., & Zhou, Z. R. (2019). Effect of perforated structure of friction block on the wear, thermal distribution and noise characteristics of railway brake systems. *Wear*, *426*, 1176–1186. https://doi.org/10.1016/j.wear.2019.01.016

Tonazzi, D., Massi, F., Baillet, L., Brunetti, J., & Berthier, Y. (2018). Interaction between contact behaviour and vibrational response for dry contact system. *Mechanical Systems and Signal Processing*, *110*, 110–121. https://doi.org/10.1016/j.ymssp.2018.03.020

Walia, M. S., Vernersson, T., Lundén, R., Blennow, F., & Meinel, M. (2019). Temperatures and wear at railway tread braking: Field experiments and simulations. *Wear*, *440*, 203086. https://doi.org/10.1016/j.wear.2019.203086

Wójcik, A., Frączek, J., & Niemczewska-Wójcik, M. (2020). The relationship between static and kinetic friction for plant granular materials. *Powder Technology*, *361*, 739–747. https://doi.org/10.1016/j.powtec.2019.11.048

Xiang, Z. Y., Mo, J. L., Ouyang, H., Massi, F., Tang, B., & Zhou, Z. R. (2020). Contact behaviour and vibrational response of a high-speed train brake friction block. *Tribology International*, *152*, 106540. https://doi.org/10.1016/j.triboint.2020.106540

Zhao, W., Wu, G., Wang, C., Yu, L., & Li, Y. (2019). Energy transfer and utilization efficiency of regenerative braking with hybrid energy storage system. *Journal of Power Sources*, *427*, 174–183. https://doi.org/10.1016/j.jpowsour.2019.04.083

